


Article

# A Novel Ruthenium(II) Polypyridyl Complex Bearing 1,8-Naphthyridine as a High Selectivity and Sensitivity Fluorescent Chemosensor for Cu<sup>2+</sup> and Fe<sup>3+</sup> Ions

Chixian He <sup>1,2</sup> , Shiwen Yu <sup>2</sup>, Shuye Ma <sup>3</sup>, Zining Liu <sup>1</sup>, Lifeng Yao <sup>2</sup>, Feixiang Cheng <sup>1,2,\*</sup> and Pinhua Liu <sup>2</sup>

- <sup>1</sup> Center for Yunnan-Guizhou Plateau Chemical Functional Materials and Pollution Control, Qujing Normal University, Qujing 655011, China; cxhe@mail.qjnu.edu.cn (C.H.); LZning151@163.com (Z.L.)
- <sup>2</sup> College of Chemistry and Environmental Science, Qujing Normal University, Qujing 655011, China; zlq9941@163.com (S.Y.); leoyao1982@163.com (L.Y.); lph13099867071@sina.com (P.L.)
- <sup>3</sup> Department of Medicine, Qujing Qilin Vocational and Technical School, Qujing 655000, China; msy\_1009@163.com
- \* Correspondence: chengfx2019@163.com; Tel.: +86-0874-099-8658

Academic Editors: Victor Mamane and John S. Fossey

Received: 26 September 2019; Accepted: 31 October 2019; Published: 7 November 2019



**Abstract:** A novel ruthenium(II) polypyridyl complex bearing 1,8-naphthyridine was successfully designed and synthesized. This complex was fully characterized by EI-HRMS, NMR, and elemental analyses. The recognition properties of the complex for various metal ions were investigated. The results suggested that the complex displayed high selectivity and sensitivity for Cu<sup>2+</sup> and Fe<sup>3+</sup> ions with good anti-interference in the CH<sub>3</sub>CN/H<sub>2</sub>O (1:1, *v/v*) solution. The fluorescent chemosensor showed obvious fluorescence quenching when the Cu<sup>2+</sup> and Fe<sup>3+</sup> ions were added. The detection limits of Cu<sup>2+</sup> and Fe<sup>3+</sup> were 39.9 nmol/L and 6.68 nmol/L, respectively. This study suggested that this Ru(II) polypyridyl complex can be used as a high selectivity and sensitivity fluorescent chemosensor for Cu<sup>2+</sup> and Fe<sup>3+</sup> ions.

**Keywords:** Ru(II) polypyridyl complex; 1,8-naphthyridine; fluorescence; chemosensor; Cu<sup>2+</sup>; Fe<sup>3+</sup>

## 1. Introduction

With the development of agriculture and industry, the application of heavy and transition metals becomes more and more prevalent, which leads to these kinds of metal ions entering ecological and environmental systems. These metal ions have posed significant damage to living organisms even at per million concentrations due to their toxicity, accumulation, and low rate of clearance, especially to the health of human beings [1–4]. Among these metal ions, Fe<sup>3+</sup> is the most abundant essential trace element in the organism. It is involved in several biological processes, such as oxygen transport, cellular respiration, enzymatic catalysis regulation of transcription, DNA repair [5–8], and so on. Similarly, Cu<sup>2+</sup> is another indispensable element in the human body after Fe<sup>3+</sup>. It is required for a number of physiological activities of the organism including enzymatic catalysis, nerve conduction, and hematopoiesis. Either the deficiency or excess of Fe<sup>3+</sup> and Cu<sup>2+</sup> can disturb the balance of cellular systems and metabolism. For example, exposure to high levels of Fe<sup>3+</sup> and Cu<sup>2+</sup> can cause many diseases, such as Menkes disease, Alzheimer's disease, Wilson disease, gastrointestinal disorders, kidney damage, hepatitis, cancer, and neurodegenerative disease [9–11]. Therefore, the detection and recognition of Fe<sup>3+</sup> and Cu<sup>2+</sup> have very important practical significance. The development of single molecular light-up probes for Fe<sup>3+</sup> and Cu<sup>2+</sup> has received increasing attention in recent years [12,13].

Wang et al. reported a rhodamine B hydrazine derivative that had a sufficiently satisfactory selective response to  $\text{Fe}^{3+}$  and  $\text{Cu}^{2+}$  [14]. Ajayakumar et al. designed and synthesized a new Rubp-Ptz in which the phenothiazine moiety was covalently linked to one of the bipyridine units of  $\text{Ru}(\text{bpy})_3^{2+}$ . Excitation of  $\text{Ru}(\text{bpy})_3^{2+}$  led to electron transfer from the phenothiazine moiety to the metal to ligand charge transfer (MLCT) excited state of  $\text{Ru}(\text{bpy})_3^{2+}$ , which resulted in efficient quenching of the luminescence. The phenothiazine moiety of Rubp-Ptz can be oxidized to a stable entity by  $\text{Cu}^{2+}$ . The new product is incapable of electron donation to the MLCT excited state of  $\text{Ru}(\text{bpy})_3^{2+}$ . The emission of the  $\text{Ru}(\text{bpy})_3^{2+}$  moiety is restored [15]. Qian et al. synthesized five coumarin derivatives, in which two compounds exhibited selectivity towards  $\text{Cu}^{2+}$  [16]. Wang et al. reported a terthiophene-derived colorimetric and fluorescent dual-channel sensor terthiophene-phenylamine TTA, which showed a significant fluorescence “turn-on” response to  $\text{Fe}^{3+}$  and an obvious fluorescence “turn-off” response to  $\text{Cu}^{2+}$  [17]. Although a large number of luminescence probes for  $\text{Fe}^{3+}$  and  $\text{Cu}^{2+}$  have been reported, most of them have disadvantages such as low sensitivity, poor selectivity, poor water solubility, and so on. Hence, the design and development of highly selective, sensitive, and water soluble chemosensors are very important.

Ru(II) complexes and in particular Ru(II) polypyridyl complexes have received much attention due to their potential application in the field of solar energy conversion [18–22], photocatalysis [23,24], water-oxidation catalyst [25,26], and luminescence sensing [27,28]. Similarly, they are applied in photodynamic therapy [29] and bio-probes [30–32] owing to their low cytotoxicity, redox stability, and water solubility.

Significant research has focused on the derivatives of 1,8-naphthyridine due to their interesting complexation properties and application. They can be used in coordination chemistry as monodentate and bidentate ligands [33]. The derivatives of 1,8-naphthyridine have been used as molecular sensor for transition and heavy metals, carboxylic acids, and guanine [34]. 1,8-Naphthyridine derivatives are remarkable fluorescent markers for nucleic acids [35,36].

Taking advantage of the excellent luminescence properties of Ru(II) polypyridyl complexes and the coordination properties of 1,8-naphthyridine derivatives, we envision that the Ru(II) polypyridyl complexes bearing 1,8-naphthyridine derivatives can also be used as molecular probes. For the aforementioned reason, we propose to synthesize a Ru(II) polypyridyl complex containing 1,8-naphthyridine derivatives. It can be used as a luminescence probe for  $\text{Fe}^{3+}$  and  $\text{Cu}^{2+}$  ions.

## 2. Experiment

### 2.1. Materials

All the solvents and reagents (analytical grade and spectroscopic grade) were purchased from reagent companies and used without further purification. 2,7-Dimethyl-1,8-naphthyridine [37,38] and *cis*- $\text{Ru}(\text{bpy})_2\text{Cl}_2 \cdot 2\text{H}_2\text{O}$  [39] were obtained according to the literature procedures.

### 2.2. Instrumentation

All of these compounds were characterized by  $^1\text{H}$ -NMR, MS, and elementary analysis. The  $^1\text{H}$ -NMR and  $^{13}\text{C}$ -NMR experiments were taken using a Mercury Plus 400 MHz spectrometer (Bruker, Karlsruhe, Germany). The chemical shifts ( $\delta$ , ppm) were acquired relative to tetramethylsilane (TMS). ESI-MS spectra were recorded by using the Bruker amaZon SL mass spectrometer (Bruker, Karlsruhe, Germany). ESI-HRMS spectra were taken on a Bruker Daltonics APEXII47e mass spectrometer (Bruker, Karlsruhe, Germany). The C, H, and N microanalyses were carried out on a Perkin-Elmer 240C analytical instrument (PerkinElmer, Norwalk, CT, USA). FTIR spectra were taken in the range of 4000–400  $\text{cm}^{-1}$  on a Thermo Nicolet AVATAR 360 FTIR spectrometer (Thermo Fisher Scientific, Waltham, MA, USA) using KBr pellets. Electronic absorption spectra and emission spectra were taken on a Varian Cary-100 UV-Visible spectrophotometer (Varian, Palo Alto, CA, USA) and a Hitachi F-4600 fluorescence spectrophotometer (Hitachi, Tokyo, Japan), respectively, using a

10 mm path length colorimetric ware. All theoretical calculations were taken using the Gaussian 09 program package in this study (Gaussian, Wallingford, CT, USA). The structure of complex  $[\{\text{Ru}(\text{bpy})_2\}_2(\mu_2\text{-H}_2\text{L})](\text{PF}_6)_4$  was optimized using the Becke-3-Lee-Yang-Parr in conjunction with the 6-311+G\* basis set for C, N, and H atoms and the LANL2DZ inclusion effective core potential (ECP) for the ruthenium atom [40]. All the optimized stationary points were identified as minima (zero imaginary frequencies) via the vibrational analyses at the same level.

### 2.3. Synthesis of 1,8-Naphthyridine-2,7-Dicarbaldehyde

1,8-Naphthyridine-2,7-dicarbaldehyde was synthesized with a minor change according to the literature [37,41]. A mixture of selenium dioxide (1.11 g, 10 mmol) in anhydrous 1,4-dioxane (10 mL) was heated to 110 °C under a nitrogen atmosphere, then 2,7-dimethyl-1,8-naphthyridine was added (316 mg, 2.0 mmol). Stirring was continued for two hours and hot filtered. Chloroform (25 mL) was added to the filtrate and washed with water (3 × 10 mL). The combined organic was washed with 5% sodium bicarbonate (aq) (25 mL), dried over anhydrous  $\text{Na}_2\text{SO}_4$ , and concentrated in vacuo. This residue was redissolved in hot ethyl acetate (25 mL), hot filtered, giving a pale brown powder. Yield: 214 mg (58%).  $^1\text{H-NMR}$  (400 MHz,  $\text{DMSO-}d_6$ )  $\delta$  = 8.28 (d,  $J$  = 8.0 Hz, 2H), 8.52 (d,  $J$  = 8.0 Hz, 2H), 10.40 (s, 2H).

### 2.4. Synthesis of Compound L

A mixture of 5-amino-1,10-phenanthroline (585 mg, 3.0 mmol) and 1,8-naphthyridine-2,7-dicarbaldehyde (186 mg, 1.0 mmol) in anhydrous EtOH (80 mL) was heated at 80 °C, then 10 drops of HOAc were added. The mixture was refluxed for 24 h. A suspension was obtained. The yellow precipitate was collected by filtration, washed with hot EtOH, and dried in vacuo. Yield: 463 mg (88%) of a yellow solid.  $^1\text{H-NMR}$  (400 MHz,  $\text{DMSO-}d_6$ )  $\delta$  = 7.79–7.91 (m, 6H), 8.55–8.57 (m, 2H), 8.76–8.79 (m, 6H), 8.96–8.99 (m, 2H), 9.13–9.17 (m, 4H), 9.24–9.26 (m, 2H). ESI-MS  $m/z$  = 540.65  $[\text{M} + \text{H}]^+$ , 562.21  $[\text{M} + \text{Na}]^+$ . Theoretical exact mass:  $m/z$  = 540.18  $[\text{M} + \text{H}]^+$ , 563.17  $[\text{M} + \text{Na}]^+$ . Found: C, 74.4; H, 3.8; N, 20.8. Calculated for  $\text{C}_{34}\text{H}_{20}\text{N}_8$ : C, 74.5; H, 3.7; N, 20.7%.

### 2.5. Synthesis of $\text{H}_2\text{L}$

L (324 mg, 0.60 mmol) was dissolved in anhydrous  $\text{CHCl}_3\text{-EtOH}$  (200 mL, 1:1,  $v/v$ ), in which  $\text{NaBH}_4$  (228 mg, 6.0 mmol) was added. The solvent was stirred at room temperature for 72 h, then washed with distilled water (50 mL × 3). The combined aqueous layers were extracted with  $\text{CH}_2\text{Cl}_2$ , then the combined organic layers were dried over anhydrous  $\text{Na}_2\text{SO}_4$ . The organic solvent was evaporated in vacuo, then the crude product was purified by column chromatography on  $\text{SiO}_2$  (eluent:  $v(\text{CH}_2\text{Cl}_2)/v(\text{EtOH}) = 10:1$ ), giving a yellow solid. Yield: 130 mg (40%).  $^1\text{H-NMR}$  (400 MHz,  $\text{DMSO-}d_6$ )  $\delta$  = 5.03 (s, 4H), 6.7 (s, 2H), 7.37 (s, 2H), 7.47 (dd,  $J$  = 4.0, 8.0 Hz, 2H), 7.73–7.78 (m, 4H), 7.95 (d,  $J$  = 8.0 Hz, 2H), 8.21 (d,  $J$  = 8.0 Hz, 2H), 8.78 (d,  $J$  = 4.0, 2H), 8.90 (d,  $J$  = 8.0 Hz, 2H), 9.16 (d,  $J$  = 4.0 Hz, 2H). ESI-MS  $m/z$  = 544.64  $[\text{M} + \text{H}]^+$ . Theoretical exact mass:  $m/z$  = 544.21  $[\text{M} + \text{H}]^+$ . Found: C, 75.1; H, 5.3; N, 19.6. Calculated for  $\text{C}_{34}\text{H}_{24}\text{N}_8$ : C, 75.0; H, 4.4; N, 20.6%.

### 2.6. Synthesis of $[\{\text{Ru}(\text{bpy})_2\}_2(\mu_2\text{-H}_2\text{L})](\text{PF}_6)_4$

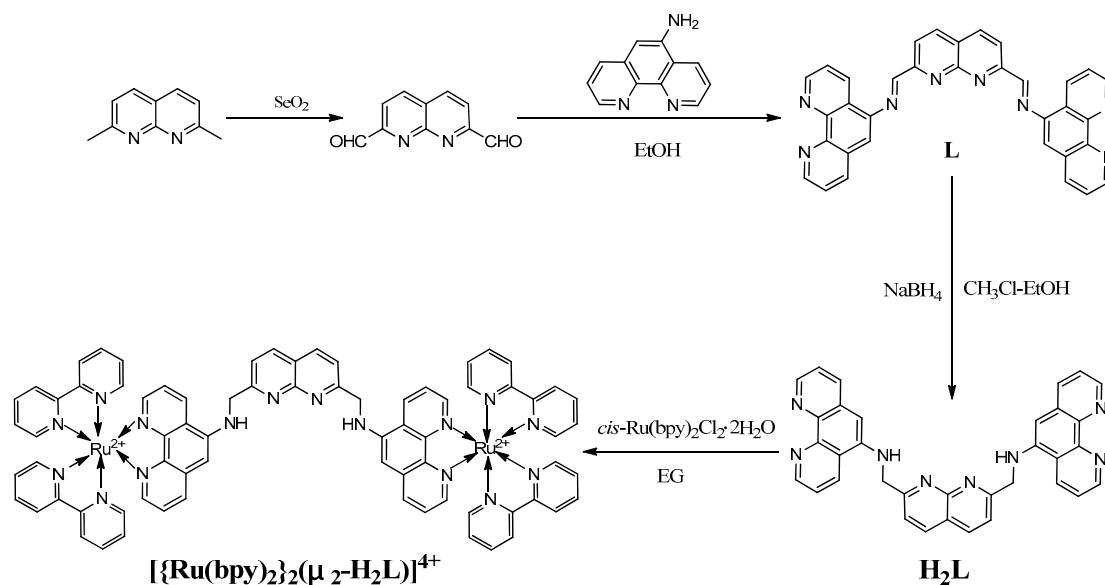
Under a nitrogen atmosphere, a mixture of *cis*- $\text{Ru}(\text{bpy})_2\text{Cl}_2 \cdot 2\text{H}_2\text{O}$  (207 mg, 0.40 mmol) and  $\text{H}_2\text{L}$  (107 mg, 0.20 mmol) in 100 mL ethylene glycol in a three necked flask was heated to 150 °C for 12 h to give a deep red solution. The solvent was evaporated in vacuo. The crude product was purified twice by column chromatography on  $\text{Al}_2\text{O}_3$ , first using  $\text{CH}_3\text{CN}$  and EtOH (8:1,  $v/v$ ) as the eluant, then using EtOH to obtain the complex  $[\{\text{Ru}(\text{bpy})_2\}_2(\mu_2\text{-H}_2\text{L})]\text{Cl}_4$ . This complex was dissolved in a minimum amount of water, then the saturated aqueous  $\text{NH}_4\text{PF}_6$  was added. The product was collected by vacuum filtration and recrystallized from an acetone/diethyl ether mixture, giving a deep red powder. Yield: 117 mg (30%).  $^1\text{H-NMR}$  (400 MHz,  $\text{DMSO-}d_6$ )  $\delta$  = 4.98 (d,  $J$  = 4.0 Hz, 4H), 6.94 (s, 2H), 7.37 (t,  $J$  = 8.0 Hz, 4H), 7.53–7.63 (m, 12H), 7.75 (d,  $J$  = 8.0 Hz, 2H), 7.80 (d,  $J$  = 4.0 Hz, 2H), 7.85 (d,  $J$  =

4.0 Hz, 2H), 7.90–7.94 (m, 2H), 8.10–8.14 (m, 6H), 8.18–8.24 (m, 6H), 8.31 (s, 2H), 8.43 (d,  $J = 8.0$  Hz, 2H), 8.82–8.90 (m, 8H), 9.11 (d,  $J = 8.0$  Hz, 2H).  $^{13}\text{C-NMR}$  (400 MHz,  $\text{DMSO-}d_6$ )  $\delta = 49.6, 124.4, 124.9, 125.7, 126.7, 128.3, 131.9, 132.9, 134.2, 138.2, 138.4, 138.8, 141.5, 147.2, 148.2, 151.7, 151.9, 152.0, 152.5, 157.0, 157.1, 157.3, 163.4$ . ESI-HRMS:  $m/z = 343.0735$   $[\text{M} - 4\text{PF}_6]^{4+}$ ,  $505.7527$   $[\text{M} - 3\text{PF}_6]^{3+}$ ,  $831.1112$   $[\text{M} - 2\text{PF}_6]^{2+}$ ,  $1087.1864$   $[\text{M} - \text{PF}_6]^+$ . Theoretical exact mass for  $\text{C}_{74}\text{H}_{56}\text{F}_{24}\text{N}_{16}\text{P}_4\text{Ru}_2$ :  $m/z = 343.0737$   $[\text{M} - 4\text{PF}_6]^{4+}$ ,  $505.7535$   $[\text{M} - 3\text{PF}_6]^{3+}$ ,  $831.1132$   $[\text{M} - 2\text{PF}_6]^{2+}$ ,  $1086.1885$   $[\text{M} - \text{PF}_6]^+$ . Found: C, 65.1; H, 4.0; N, 16.7. Calculated for  $\text{C}_{74}\text{H}_{56}\text{F}_{24}\text{N}_{16}\text{P}_4\text{Ru}_2$ : C, 64.81; H, 4.1; N, 16.34%. IR (KBr,  $\text{cm}^{-1}$ ) 3445br 1624m, 1528m, 1465m, 1434m, 1312w, 1241w, 1169w, 1047w, 837s, 764m, 728w, 558m.

### 3. Result and Discussion

#### 3.1. Synthesis

A novel dinuclear Ru(II) polypyridyl complex containing 1,8-naphthyridine was first designed and synthesized. The target complex was prepared in four steps (Scheme 1). The starting material 2,7-methyl-1,8-naphthyridine was synthesized according to the literature [37,38]. In the first step, 2,7-methyl-1,8-naphthyridine was oxidized to dialdehyde by the selenium dioxide. The Schiff base was obtained in good yield with the reaction of dialdehyde and 5-amino-1,10-phenanthroline. The Schiff base was then reduced by sodium borohydride to give the ligand  $\text{H}_2\text{L}$ . All the organic compounds were purified by column chromatography.  $\text{cis-}[\text{Ru}(\text{bpy})_2\text{Cl}_2]\cdot\text{H}_2\text{O}$  reacted with the ligand  $\text{H}_2\text{L}$  to give the complex  $[\{\text{Ru}(\text{bpy})_2\}_2(\mu_2\text{-H}_2\text{L})]\text{Cl}_4$ . Then, the  $\text{Cl}^-$  ion of  $[\{\text{Ru}(\text{bpy})_2\}_2(\mu_2\text{-H}_2\text{L})]\text{Cl}_4$  was exchanged by the  $\text{PF}_6^-$  of saturated aqueous  $\text{NH}_4\text{PF}_6$  to obtain  $[\{\text{Ru}(\text{bpy})_2\}_2(\mu_2\text{-H}_2\text{L})](\text{PF}_6)_4$ . The  $^1\text{H-NMR}$ ,  $^{13}\text{C-NMR}$ , and MS spectra of the complex were consistent with the expected structure.



Scheme 1. Synthesis of the ligand  $\text{H}_2\text{L}$  and Ru(II) complex.

#### 3.2. Computational Studies

The simulations of the HOMO and LUMO electron density distribution in the frontier molecular orbitals of the complex are shown in Figure 1. It was observed that the LUMO and LUMO + 1 were distributed mostly on the 2,2'-bipyridine and 1,10-phenanthroline unit and that the LUMO + 2 was localized primarily on the two 2,2'-bipyridine units, but the HOMO orbital had amplitudes on the 1,10-phenanthroline unit in one of the Ru centers. The electron distribution of HOMO and LUMO provided strong evidence of the photoinduced electron transfer (PET) process in the new complexes [42–44].

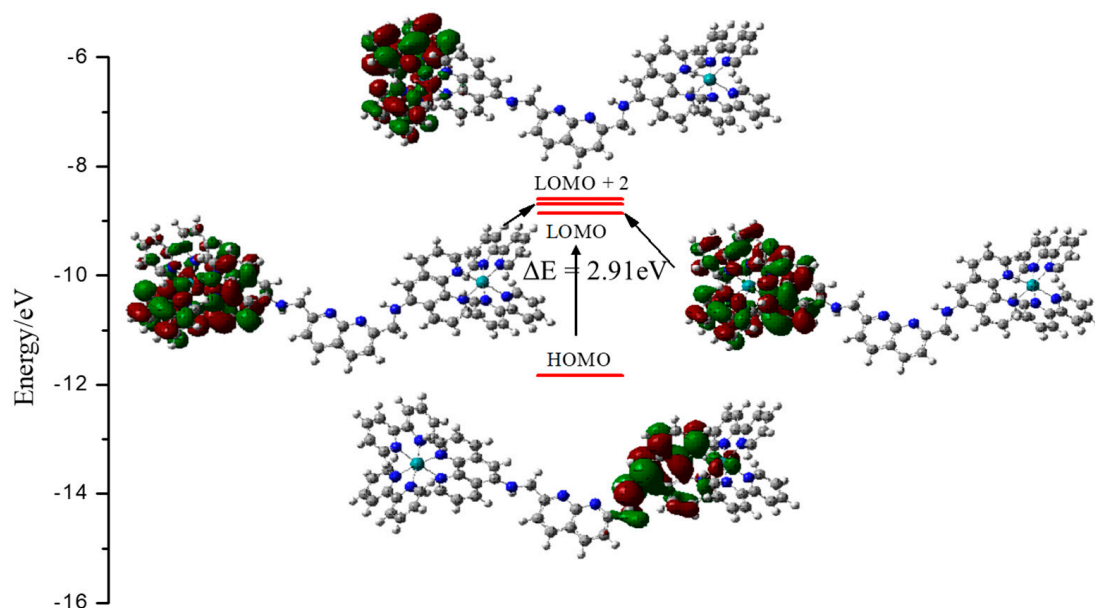


**Figure 1.** Electron distribution and energy diagram of HOMO and LUMO orbitals for the complex  $[\text{Ru}(\text{bpy})_2]_2(\mu_2\text{-H}_2\text{L})^{4+}$ .

### 3.3. Selectivity of Complex to Metal Ions

The selectivity of the complex to metal ions was evaluated with fluorescence experiments. The fluorescence experiments were recorded with a concentration of  $10^{-5}$  mol/L in the presence of tetrabutyl perchlorate amine (TBAP, 0.1 mol/L) in  $\text{CH}_3\text{CN}/\text{H}_2\text{O}$  (1:1, *v/v*) at room temperature, then 5.0 equivalents of nitrate or perchlorate salts of metal ions ( $\text{Ag}^+$ ,  $\text{Ca}^{2+}$ ,  $\text{Co}^{2+}$ ,  $\text{Ba}^{2+}$ ,  $\text{Cr}^{3+}$ ,  $\text{Cd}^{2+}$ ,  $\text{Ni}^{2+}$ ,  $\text{Li}^+$ ,  $\text{Na}^+$ ,  $\text{Mg}^{2+}$ ,  $\text{Zn}^{2+}$ ,  $\text{Mn}^{2+}$ ,  $\text{Fe}^{3+}$ ,  $\text{Fe}^{2+}$ ,  $\text{Pb}^{2+}$ ,  $\text{Hg}^{2+}$ , and  $\text{Cu}^{2+}$ ) were added to the solution, respectively. The fluorescence properties are recorded and compared in Figure 2. As shown in Figure 2, the complex showed a strong fluorescence at 612 nm. However, the fluorescence of the solution was quenched to 48 a.u. and 23 a.u., respectively, when  $\text{Cu}^{2+}$  and  $\text{Fe}^{3+}$  were added. The quenching of the fluorescence intensities with  $\text{Pb}^{2+}$  and  $\text{Hg}^{2+}$  was small. All other metal ions tested did not cause any significant change to the luminescence intensity of the solution. The phenomena of the fluorescence indicated that the complex had a selectivity for  $\text{Cu}^{2+}$  and  $\text{Fe}^{3+}$  ions. Therefore, it can be used as a “turn-off” fluorescent chemosensor for  $\text{Cu}^{2+}$  and  $\text{Fe}^{3+}$  in the  $\text{CH}_3\text{CN}/\text{H}_2\text{O}$  media. This dramatic quenching of the initial luminescence of RuL induced by  $\text{Cu}^{2+}$  and  $\text{Fe}^{3+}$  was due to the reverse photoinduced electron transfer (PET) from the 2,2'-bipyridine ruthenium (II) moieties to the 1,8-naphthyridine nitrogen atom because of the decrease in the electron density upon  $\text{Cu}^{2+}$  and  $\text{Fe}^{3+}$  complexation [45]. In order to further evaluate the selectivity of  $[\text{Ru}(\text{bpy})_2]_2(\mu_2\text{-H}_2\text{L})(\text{PF}_6)_4$  for detecting  $\text{Cu}^{2+}$  and  $\text{Fe}^{3+}$ , competitive experiments were carried out at room temperature. Five equivalents of  $\text{Cu}^{2+}$  and  $\text{Fe}^{3+}$  were added to the solution of the complex ( $\text{CH}_3\text{CN}/\text{H}_2\text{O} = 1:1, v/v$ ), respectively. Then, the other metal ions ( $\text{Ag}^+$ ,  $\text{Ca}^{2+}$ ,  $\text{Co}^{2+}$ ,  $\text{Ba}^{2+}$ ,  $\text{Cr}^{3+}$ ,  $\text{Cd}^{2+}$ ,  $\text{Ni}^{2+}$ ,  $\text{Li}^+$ ,  $\text{Na}^+$ ,  $\text{Mg}^{2+}$ ,  $\text{Zn}^{2+}$ ,  $\text{Mn}^{2+}$ ,  $\text{Fe}^{2+}$ ,  $\text{Pb}^{2+}$ ,  $\text{Hg}^{2+}$ ) were added to the mixed solution, respectively (Figure 3; Figure 4). As shown in Figures 3 and 4, the fluorescence of the complex with  $\text{Cu}^{2+}$  had no obvious influence when the other metal ions existed in the system. However,  $\text{Ca}^{2+}$ ,  $\text{Cr}^{3+}$ , and  $\text{Zn}^{2+}$  had a small influence, and the other ions had no obvious influence in the  $\text{Fe}^{3+}$  ion experiments. Therefore, the complex can be used as an excellent fluorescent chemosensor for detecting  $\text{Cu}^{2+}$  and  $\text{Fe}^{3+}$  ions [14,46].

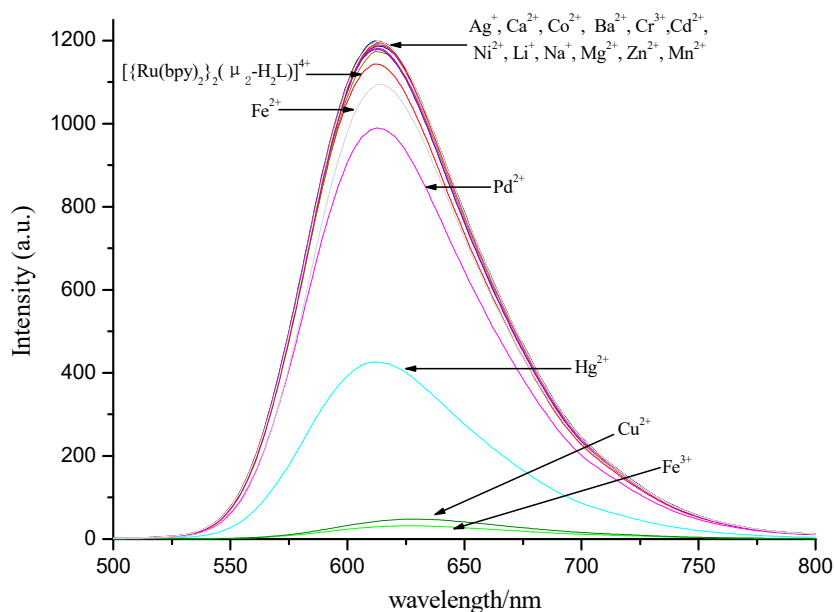


**Figure 2.** Fluorescence spectra of the complex  $[\text{Ru}(\text{bpy})_2]_2(\mu_2\text{-H}_2\text{L})^{4+}$  ( $10^{-5}$  mol/L in  $\text{CH}_3\text{CN}/\text{H}_2\text{O} = 1:1$ ,  $v/v$ , excitation wavelength = 450 nm) upon the addition of 5.0 equivalents of various metal ions at room temperature.

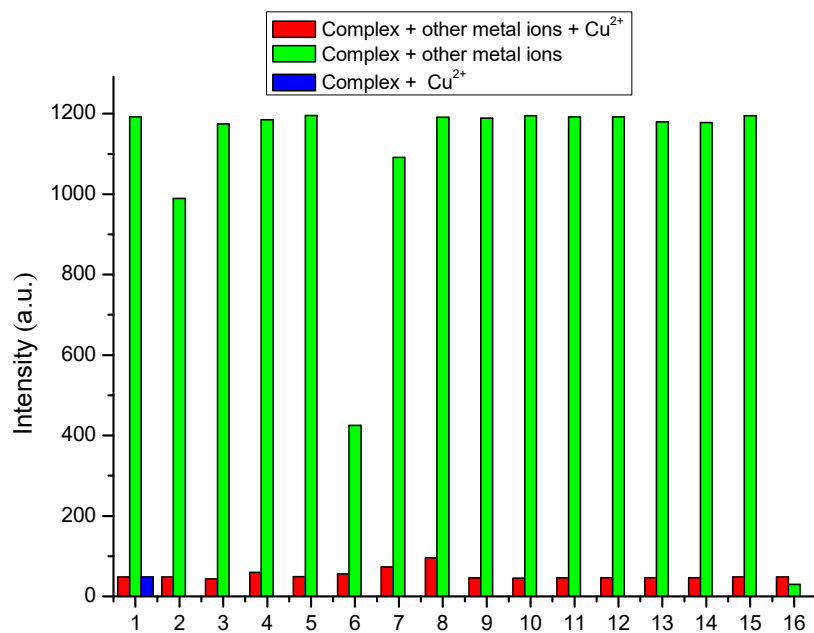


**Figure 3.** Changes in the fluorescence intensity of the complex  $[\text{Ru}(\text{bpy})_2]_2(\mu_2\text{-H}_2\text{L})^{4+}$  ( $10^{-5}$  mol/L in  $\text{CH}_3\text{CN}/\text{H}_2\text{O} = 1:1$ ,  $v/v$ , excitation wavelength = 450 nm) upon the addition of  $\text{Cu}^{2+}$  in the presence of other metal ions. The red bars represent the fluorescence intensity of  $[\text{Ru}(\text{bpy})_2]_2(\mu_2\text{-H}_2\text{L})^{4+}$  upon the addition of 5.0 equiv. of  $\text{Cu}^{2+}$  in the presence of: 1  $\text{Cd}^{2+}$ , 2  $\text{Pb}^{2+}$ , 3  $\text{Ca}^{2+}$ , 4  $\text{Mg}^{2+}$ , 5  $\text{Zn}^{2+}$ , 6  $\text{Hg}^{2+}$ , 7  $\text{Fe}^{2+}$ , 8  $\text{Ba}^{2+}$ , 9  $\text{Ni}^{2+}$ , 10  $\text{Li}^+$ , 11  $\text{Mn}^{2+}$ , 12  $\text{Cr}^{3+}$ , 13  $\text{Na}^+$ , 14  $\text{Co}^{2+}$ , 15  $\text{Ag}^+$ , 16  $\text{Fe}^{3+}$ ; the green bars represent the changes in the fluorescence intensity of  $[\text{Ru}(\text{bpy})_2]_2(\mu_2\text{-H}_2\text{L})^{4+}$  upon the addition of other metal ions, respectively. The blue bar represents the fluorescence intensity of  $[\text{Ru}(\text{bpy})_2]_2(\mu_2\text{-H}_2\text{L})^{4+}$  when 5.0 equiv. of  $\text{Cu}^{2+}$  were added.

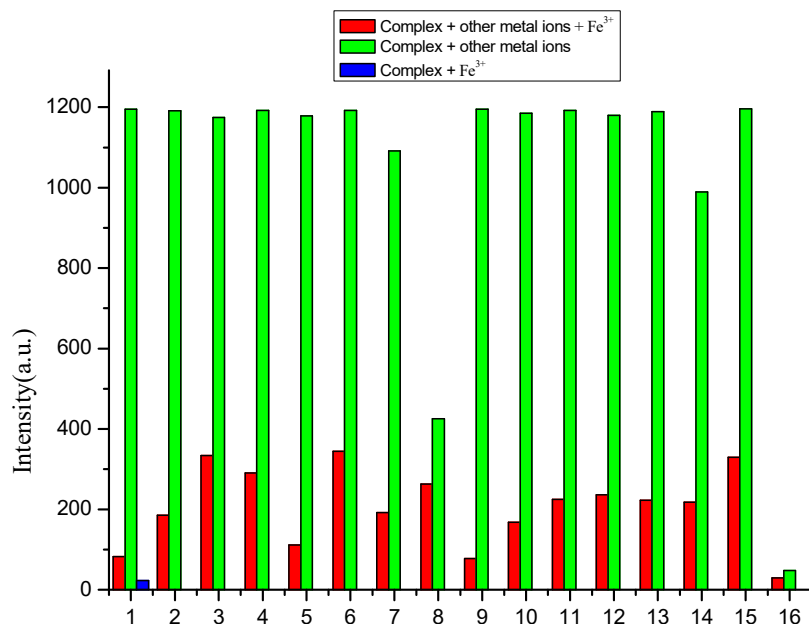


**Figure 4.** Changes in the fluorescence intensity of the complex  $[\{\text{Ru}(\text{bpy})_2\}_2(\mu_2\text{-H}_2\text{L})]^{4+}$  ( $10^{-5}$  mol/L in  $\text{CH}_3\text{CN}/\text{H}_2\text{O} = 1:1$ ,  $v/v$ , excitation wavelength = 450 nm) toward  $\text{Fe}^{3+}$  in the presence of other metal ions. The red bars represent the fluorescence intensity of  $[\{\text{Ru}(\text{bpy})_2\}_2(\mu_2\text{-H}_2\text{L})]^{4+}$  when 5.0 equiv. of  $\text{Fe}^{3+}$  were added in the presence of: 1  $\text{Ag}^+$ , 2  $\text{Ba}^{2+}$ , 3  $\text{Ca}^{2+}$ , 4  $\text{Cd}^{2+}$ , 5  $\text{Co}^{2+}$ , 6  $\text{Cr}^{3+}$ , 7  $\text{Fe}^{2+}$ , 8  $\text{Hg}^{2+}$ , 9  $\text{Li}^+$ , 10  $\text{Mg}^{2+}$ , 11  $\text{Mn}^{2+}$ , 12  $\text{Na}^+$ , 13  $\text{Ni}^{2+}$ , 14  $\text{Pb}^{2+}$ , 15  $\text{Zn}^{2+}$ , 16  $\text{Cu}^{2+}$ ; the green bars represent the changes in fluorescence intensity of  $[\{\text{Ru}(\text{bpy})_2\}_2(\mu_2\text{-H}_2\text{L})]^{4+}$  when other metal ions were added, respectively. The blue bar represents the fluorescence intensity of  $[\{\text{Ru}(\text{bpy})_2\}_2(\mu_2\text{-H}_2\text{L})]^{4+}$  when 5.0 equiv. of  $\text{Fe}^{3+}$  were added.

### 3.4. Sensitivity of Complex to $\text{Cu}^{2+}$ and $\text{Fe}^{3+}$ Ions

Fluorescence titration experiments for the complex with the progressive addition of  $\text{Cu}^{2+}$  and  $\text{Fe}^{3+}$  ions were carried out. As shown in Figures 5 and 6, the fluorescence intensity of the complex gradually decreased at 612 nm with an increasing concentration of  $\text{Cu}^{2+}$  and  $\text{Fe}^{3+}$  ions from 0 to 1.5 equivalents. The metal ions combined with the complex  $[\{\text{Ru}(\text{bpy})_2\}_2(\mu_2\text{-H}_2\text{L})](\text{PF}_6)_4$ , which made the electron transfer process easier than in the complex  $[\{\text{Ru}(\text{bpy})_2\}_2(\mu_2\text{-H}_2\text{L})](\text{PF}_6)_4$  [46–48]. There was a good linear relationship between the fluorescence intensity and the concentration of  $\text{Cu}^{2+}$  ions with the correlation coefficient of  $R = 0.9987$  when the concentration of  $\text{Cu}^{2+}$  varied from  $5 \times 10^{-7}$  mol/L to  $10^{-5}$  mol/L (Figure 7). There was a linear relationship between the fluorescence intensity and the concentration of  $\text{Fe}^{3+}$  ions with the correlation coefficient of  $R = 0.9501$  when the concentration of  $\text{Fe}^{3+}$  varied from  $6.25 \times 10^{-6}$  mol/L to  $8.0 \times 10^{-6}$  mol/L (Figure 8). Furthermore, the equation:  $3\sigma/k$  (where  $\sigma$  is the standard deviation of blank measurements,  $k$  is the slope between intensity vs. the concentration of ions) was used to obtain the detection limit of  $\text{Cu}^{2+}$  and  $\text{Fe}^{3+}$  [48,49]. The detection limits of  $\text{Cu}^{2+}$  and  $\text{Fe}^{3+}$  were 39.9 nmol/L and 6.68 nmol/L, which were far lower than the maximum allowable level of the WHO for drinking water. The results suggested that the complex was potentially applicable for quantitative analysis of  $\text{Cu}^{2+}$  and  $\text{Fe}^{3+}$  ions in environmental and biological systems.

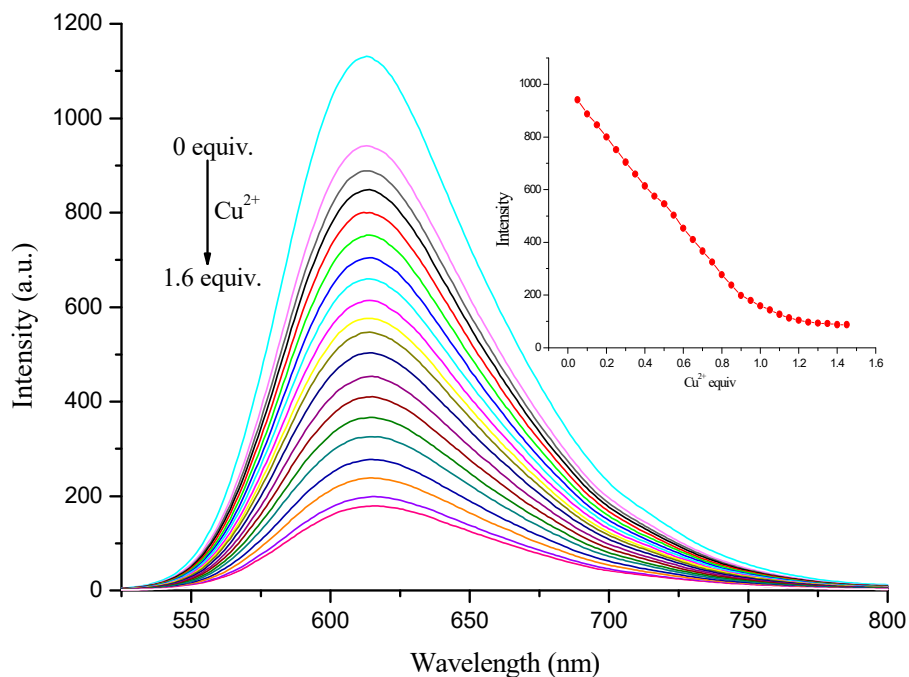


**Figure 5.** Emission spectra of the complex  $[\text{Ru}(\text{bpy})_2]_2(\mu_2\text{-H}_2\text{L})(\text{PF}_6)_4$  ( $10^{-5}$  mol/L in  $\text{CH}_3\text{CN}/\text{H}_2\text{O} = 1:1, v/v$ , excitation wavelength = 450 nm) upon the addition of  $\text{Cu}(\text{ClO}_4)_2$  (0–1.0 equiv.) at room temperature; the plot of emission intensity at 612 nm vs. the added  $\text{Cu}^{2+}$  equivalents is shown in the inset.

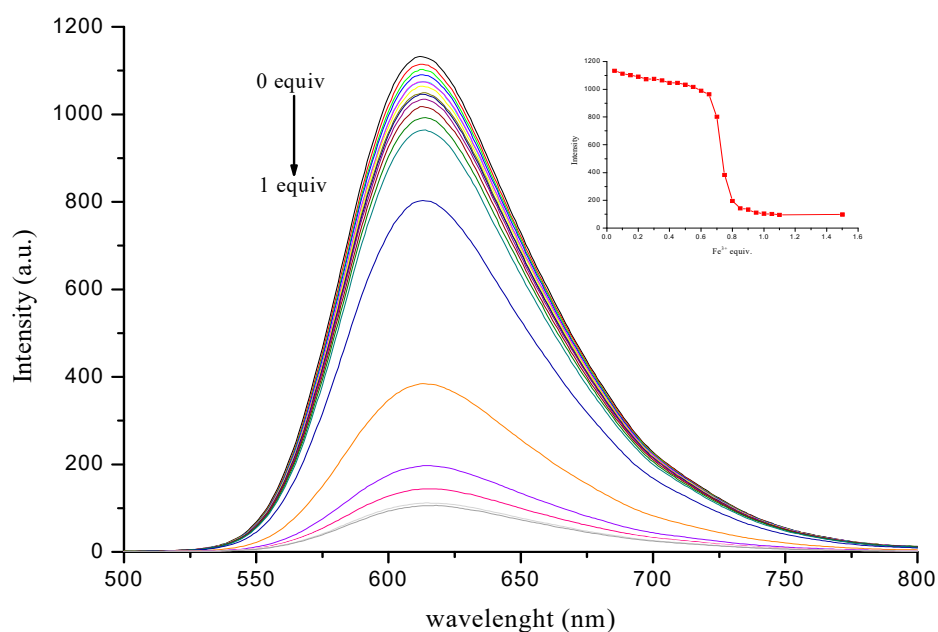


**Figure 6.** Emission spectra of the complex  $[\text{Ru}(\text{bpy})_2]_2(\mu_2\text{-H}_2\text{L})(\text{PF}_6)_4$  ( $10^{-5}$  mol/L in  $\text{CH}_3\text{CN}/\text{H}_2\text{O} = 1:1, v/v$ , excitation wavelength = 450 nm) upon the addition of  $\text{Fe}(\text{ClO}_4)_3$  (0–1.6 equiv.) at room temperature; the plot of emission intensity at 612 nm vs. the added  $\text{Fe}^{3+}$  equivalents is shown in the inset.



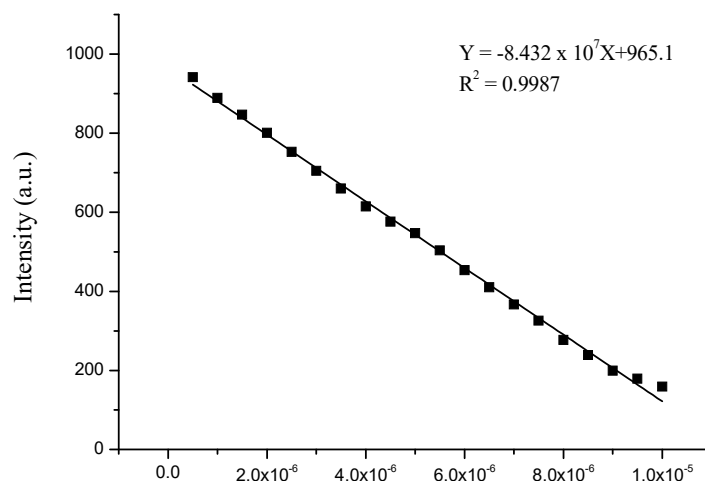


Figure 7. Plot of linear fitting for emission intensity vs. the concentration of  $\text{Cu}^{2+}$  (mol/L).

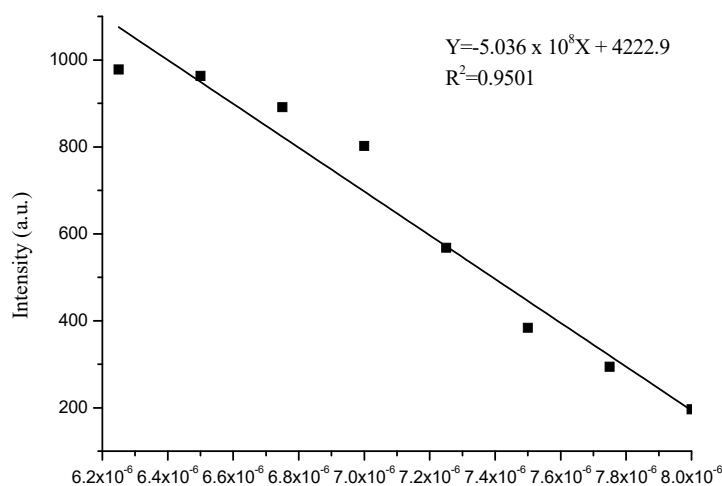
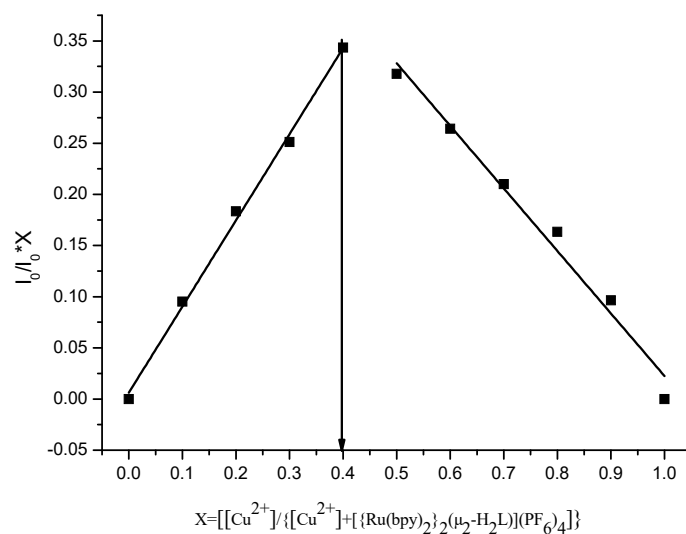


Figure 8. Plot of linear fitting for emission intensity vs. the concentration of  $\text{Fe}^{3+}$  (mol/L).

### 3.5. Mode of Binding with $\text{Cu}^{2+}$ and $\text{Fe}^{3+}$

In order to explore the binding stoichiometry of  $\text{Cu}^{2+}$  and  $\text{Fe}^{3+}$  with  $[\{\text{Ru}(\text{bpy})_2\}_2(\mu_2\text{-H}_2\text{L})](\text{PF}_6)_4$ , Job's plot analyses were used to determine binding stoichiometries. The analysis results suggested that  $[\{\text{Ru}(\text{bpy})_2\}_2(\mu_2\text{-H}_2\text{L})](\text{PF}_6)_4$  binds with  $\text{Cu}^{2+}$  and  $\text{Fe}^{3+}$  in 3:2 and 1:1 stoichiometry ratios, respectively (Figures 9 and 10). The ESI-MS experiments were further carried out by adding 2.0 equivalents of  $\text{Cu}^{2+}$  and  $\text{Fe}^{3+}$  to the acetonitrile solution of  $[\{\text{Ru}(\text{bpy})_2\}_2(\mu_2\text{-H}_2\text{L})](\text{PF}_6)_4$ , respectively (Figures S9 and S10). The peaks at  $m/z = 424.33$  and  $646.05$  were assigned to  $[\text{M} - 12\text{PF}_6 - 4\text{ClO}_4 - 6\text{H}]^{10+}$  and  $[\text{M} - 12\text{PF}_6 - \text{ClO}_4 - 6\text{H}]^{7+}$ , respectively. The calculated molecular weights of  $[\text{M} - 12\text{PF}_6 - 4\text{ClO}_4 - 6\text{H}]^{10+}$  and  $[\text{M} - 12\text{PF}_6 - \text{ClO}_4 - 6\text{H}]^{7+}$  were 423.70 and 647.65, respectively. The M was  $[\{\{\text{Ru}(\text{bpy})_2\}_2(\mu_2\text{-H}_2\text{L})\}_3\text{Cu}_2](\text{PF}_6)_{12}(\text{ClO}_4)_4$  (Figure S11a). The peaks at  $m/z = 254.40$  and  $335.41$  were attributed to  $[\text{M} - 4\text{PF}_6 - 2\text{ClO}_4]^{6+}$  and  $[\text{M} - 3\text{PF}_6 - 2\text{ClO}_4]^{5+}$ , respectively. The calculated molecular weights of  $[\text{M} - 4\text{PF}_6 - 2\text{ClO}_4]^{6+}$  and  $[\text{M} - 3\text{PF}_6 - 2\text{ClO}_4]^{5+}$  were 254.53 and 334.43. The M was  $[\{\{\text{Ru}(\text{bpy})_2\}_2(\mu_2\text{-H}_2\text{L})\}\text{Fe}](\text{PF}_6)_4(\text{ClO}_4)_3$  (Figure S11b), respectively. This indicated that the ratios of  $[\{\text{Ru}(\text{bpy})_2\}_2(\mu_2\text{-H}_2\text{L})](\text{PF}_6)_4$  bound with  $\text{Cu}^{2+}$  and  $\text{Fe}^{3+}$  were 3:2 and 1:1, respectively. The results were consistent with Job's plot analyses.



**Figure 9.** Job's plot in  $CH_3CN/H_2O$  ( $v/v$ , 1:1) of the complex  $[Ru(bpy)_2]_2(\mu_2-H_2L)(PF_6)_4$  and  $Cu^{2+}$  binding.

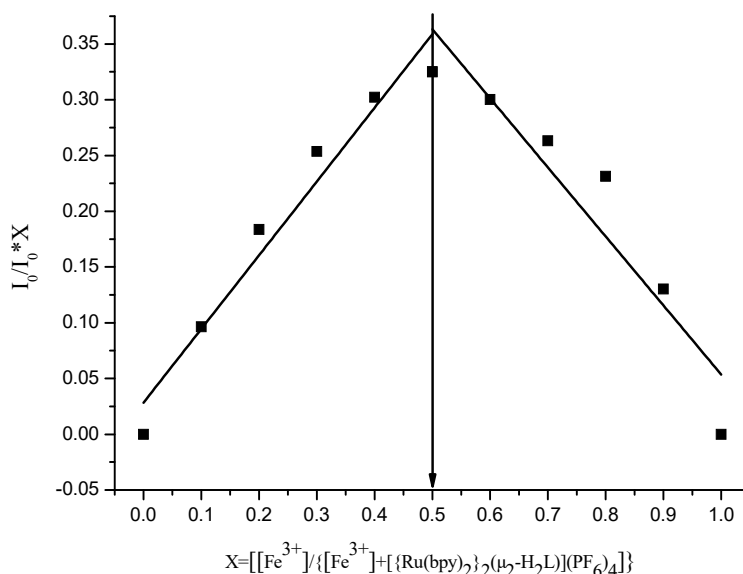


**Figure 10.** Jobs plot in  $CH_3CN/H_2O$  ( $v/v$ , 1:1) of the complex  $[Ru(bpy)_2]_2(\mu_2-H_2L)]^{4+}$  and  $Fe^{3+}$  binding.

#### 4. Conclusions

In summary, a novel fluorescent chemosensor was synthesized from 2,7-dimethyl-1,8-naphthyridine and 5-amino-1,10-phenanthroline. The  $^1H$ -NMR,  $^{13}C$ -NMR, and ESI-HRMS results were consistent with the expected structures. The recognition behaviors of  $[Ru(bpy)_2]_2(\mu_2-H_2L)(PF_6)_4$  toward the cation were investigated. The luminescence could be almost quenched by the 5.0 equivalents of  $Cu^{2+}$  or  $Fe^{3+}$  ions. Further study showed that the complex could be used as a "turn-off" fluorescent chemosensor to detect the  $Cu^{2+}$  and  $Fe^{3+}$  ions. The chemosensor showed strong anti-interference, good selectivity, and high sensitivity. The detection limits of  $Cu^{2+}$  and  $Fe^{3+}$  were 39.9 nmol/L and 6.68 nmol/L, respectively. The ESI-MS experiments indicated the modes of binding to be 3:2 and 1:1, respectively. The study provided an experimental basis for the development of  $Cu^{2+}$  or  $Fe^{3+}$  ion probes that have high sensitivity and application prospects.

**Supplementary Materials:** The following are available online. Figure S1:  $^1H$ -NMR spectrum for 1,8-naphthyridine-2,7-dicarbaldehyde (in  $CDCl_3$ ), Figure S2:  $^1H$ -NMR spectrum for L (in  $DMSO-d_6$  and a

small amount of  $\text{CDCl}_3$ ), Figure S3:  $^1\text{H-NMR}$  spectrum for  $\text{H}_2\text{L}$  (in  $\text{DMSO-}d_6$  and a small amount of  $\text{CDCl}_3$ ). Figure S4:  $^1\text{H-NMR}$  spectrum for  $[\{\text{Ru}(\text{bpy})_2\}_2(\mu_2\text{-H}_2\text{L})](\text{PF}_6)_4$  (in  $\text{DMSO-}d_6$ ), Figure S5:  $^{13}\text{C-NMR}$  spectrum for  $[\{\text{Ru}(\text{bpy})_2\}_2(\mu_2\text{-H}_2\text{L})](\text{PF}_6)_4$  (in  $\text{DMSO-}d_6$ ), Figure S6: ESI-MS for L, Figure S7: ESI-MS for  $\text{H}_2\text{L}$ , Figure S8: ESI-HRMS for  $[\{\text{Ru}(\text{bpy})_2\}_2(\mu_2\text{-H}_2\text{L})](\text{PF}_6)_4$ , Figure S9: ESI-MS for  $[\{\{\text{Ru}(\text{bpy})_2\}_2(\mu_2\text{-H}_2\text{L})\}_3\text{Cu}_2](\text{PF}_6)_{12}(\text{ClO}_4)_4$ , Figure S10: ESI-MS for  $[\{\{\text{Ru}(\text{bpy})_2\}_2(\mu_2\text{-H}_2\text{L})\}\text{Fe}](\text{PF}_6)_4(\text{ClO}_4)_3$ , Figure S11: The “sandwich” of hypothetical structures of new product of  $\text{Cu}^{2+}$  (a) and hypothetical structures of new product of  $\text{Fe}^{3+}$  (b).

**Author Contributions:** Conceptualization, C.H. and F.C.; methodology, C.H., P.L. and Z.L.; software, S.Y., L.Y. and S.M.; formal analysis, C.H., F.C. and P.L.; writing—original draft preparation, C.H.; writing—review and editing, C.H. and F.C.; funding acquisition, F.C.

**Funding:** We thank the application basis research project of Yunnan Province Science and Technology Department (2016FD079), the Scientific Research Project of Yunnan Province Education Department (2017ZDX147), and Innovative Research Team (in Science and Technology) in University of Yunnan Province (IRTSTYN) for providing the financial support.

**Conflicts of Interest:** The authors declare no conflict of interest.

## References

1. Frausto da Silva, J.; Williams, R.J.P. *The Biological Chemistry of the Elements*; Clarendon Press: Oxford, UK, 1993; p. 539.
2. Darwish, I.A.; Blake, D.A. Development and validation of a one-step immunoassay for determination of cadmium in human serum. *Anal. Chem.* **2011**, *74*, 52–58. [[CrossRef](#)] [[PubMed](#)]
3. Fang, M.; Xia, S.; Bi, J.; Travis, P.; Wigstrom, T.P.; Valenzano, L.; Wang, J.; Tanasova, M.; Rudy, L.; Luck, R.L.; et al. Detecting Zn(II) ions in live cells with near-infrared fluorescent probes. *Molecules* **2019**, *24*, 1592. [[CrossRef](#)]
4. Bi, J.; Fang, M.; Wang, J.; Xia, S.; Zhang, Y.; Zhang, J.; Vegesna, G.; Zhang, S.; Marina Tanasova, M.; Luo, F.T.; et al. Near-infrared fluorescent probe for sensitive detection of Pb(II) ions in living cells. *Inorg. Chim. Acta.* **2017**, *468*, 140–145. [[CrossRef](#)] [[PubMed](#)]
5. Liu, X.; Theil, E.C. Ferritins: Dynamic management of biological iron and oxygen chemistry. *Acc. Chem. Res.* **2005**, *38*, 167–175. [[CrossRef](#)] [[PubMed](#)]
6. Da Silvaand, J.J.R.F.; Williams, R.J.P. *In the Biological Chemistry of the Elements: The Inorganic Chemistry of Life*; Clarendon: Oxford, UK, 1991.
7. De Silva, A.P.; Gunaratne, H.Q.N.; Gunlaugsson, T.; Huxley, A.J.M.; McCoy, C.P.; Rademacher, J.T.; Rice, T.E. Signaling recognition events with fluorescent sensors and switches. *Chem. Rev.* **1997**, *97*, 1515–1566. [[CrossRef](#)] [[PubMed](#)]
8. Mense, S.M.; Zhang, L. Heme: A versatile signaling molecule controlling the activities of diverse regulators ranging from transcription factors to MAP kinases. *Cell Res.* **2006**, *16*, 681–692. [[CrossRef](#)]
9. Domink, H.; Svetlana, L. Wilson disease: Not just a copper disorder. Analysis of a Wilson disease model demonstrates the link between copper and lipid metabolism. *Mol. Biosyst.* **2007**, *3*, 816–824.
10. Georgopoulos, P.G.; Roy, A.; Yonone-Lioy, M.J.; Opiekun, R.E.; Lioy, P.J. Environmental copper: Its dynamics and human exposure issues. *J. Toxicol. Environ. Health B* **2001**, *4*, 341–394. [[CrossRef](#)]
11. Praveen, L.; Reddy, M.L.P.; Varma, R.L. Dansyl-styrylquinoline conjugate as divalent iron sensor. *Tetrahedron Lett.* **2010**, *51*, 6626–6629. [[CrossRef](#)]
12. Wang, K.P.; Lei, Y.; Zhang, S.J.; Zheng, W.J.; Chen, J.P.; Chen, S.; Hu, Z.Q. Fluorescent probe for Fe(III) with high selectivity and its application in living cells. *Sens. Actuator B-Chem.* **2017**, *252*, 1140–1145. [[CrossRef](#)]
13. Schmitteland, M.; Lin, H. Quadruple-channel sensing: A molecular sensor with a single type of receptor site for selective and quantitative multi-ion analysis. *Angew. Chem. Int. Ed.* **2007**, *46*, 893–896. [[CrossRef](#)] [[PubMed](#)]
14. Wang, L.; Ye, D.; Li, W.; Liu, Y.; Li, L.; Zhang, W.; Ni, L. Fluorescent and colorimetric detection of Fe(III) and Cu(II) by a difunctional rhodamine-based probe. *Spectrochim. Acta Part A* **2017**, *183*, 291–297. [[CrossRef](#)] [[PubMed](#)]
15. Ajayakumar, G.; Sreenath, K.; Gopidas, K.R. Phenothiazine attached  $\text{Ru}(\text{bpy})_3^{2+}$  derivative as highly selective turn-ON luminescence chemodosimeter for  $\text{Cu}^{2+}$ . *Dalton Trans.* **2009**, *21*, 1180–1186. [[CrossRef](#)] [[PubMed](#)]

16. Qian, B.; Váradi, L.; Trinchi, A.; Suzie, M.; Reichman, S.M.; Bao, L.; Lan, M.; Wei, G.; Ivan, S.; Cole, I.S. The design and synthesis of fluorescent coumarin derivatives and their study for Cu<sup>2+</sup> sensing with an application for aqueous Soil extracts. *Molecules* **2019**, *24*, 3569. [[CrossRef](#)]
17. Wang, J.; Wei, T.; Ma, F.; Li, T.; Niu, Q. A novel fluorescent and colorimetric dual-channel sensor for the fast, reversible and simultaneous detection of Fe<sup>3+</sup> and Cu<sup>2+</sup> based on terthiophene derivative with high sensitivity and selectivity. *J. Photoch. Photobiol. A* **2019**, *383*, 111982–111990. [[CrossRef](#)]
18. Kalyanasundaram, K. Photophysics, photochemistry and solar energy conversion with tris(bipyridyl)ruthenium(II) and its analogs. *Coord. Chem. Rev.* **1982**, *46*, 159–244. [[CrossRef](#)]
19. Hara, M.; Waraksa, C.C.; Lean, J.T.; Lewis, B.A.; Mallouk, T.E. Photocatalytic water oxidation in a buffered Tris(2,2'-bipyridyl) ruthenium complex-colloidal IrO<sub>2</sub> system. *J. Phys. Chem. A* **2000**, *104*, 5275–5280. [[CrossRef](#)]
20. Elmorsy, R.M.; Su, R.; Faddab, A.A.; Etmanb, H.A.; Tawfik, E.H.; El-Shafei, A. Effect of terthiophene spacer position in Ru(II) bipyridyl complexes on the photocurrent and photovoltage for high efficiency dye-sensitized solar cells. *Dyes Pigments* **2018**, *156*, 348–356. [[CrossRef](#)]
21. Medved'ko, A.V.; Ivanov, V.K.; Kiskin, M.A.; Sadovnikov, A.A.; Apostolova, E.S.; Grinberg, V.A.; Emets, V.V.; Chizhov, A.O.; Nikitin, O.M.; Magdesieva, T.V.; et al. The design and synthesis of thiophene-based ruthenium(II) complexes as promising sensitizers for dye-sensitized solar cells. *Dyes Pigments* **2017**, *140*, 169–178. [[CrossRef](#)]
22. Morita, K.; Sakai, K.; Ozawa, H. A new class of molecular-based photoelectrochemical cell for solar hydrogen production consisting of two mesoporous TiO<sub>2</sub> Electrodes. *ACS Appl. Energy Mater.* **2019**, *2*, 987–992. [[CrossRef](#)]
23. Santiago-Portillo, A.; Baldoví, H.G.; Carbonell, E.; Navalón, S.; Álvaro, M.; García, H.; Ferrer, B. Ruthenium(II) tris(2,2'-bipyridyl) complex incorporated in UiO-67 as photoredox catalyst. *J. Phys. Chem. C* **2018**, *122*, 29190–29199. [[CrossRef](#)]
24. Li, X.; Hao, Z.; Zhang, F.; Li, H. Reduced graphene oxide-immobilized tris(bipyridine) ruthenium(II) complex for efficient visible-light-driven reductive dehalogenation reaction. *ACS Appl. Mater. Interfaces* **2016**, *8*, 12141–12148. [[CrossRef](#)] [[PubMed](#)]
25. Tong, L.; Thummel, R.P. Mononuclear ruthenium polypyridine complexes that catalyze water oxidation. *Chem. Sci.* **2016**, *7*, 6591–6603. [[CrossRef](#)] [[PubMed](#)]
26. Rabten, W.; Kärkaäs, M.D.; Åkermark, T.; Chen, H.; Liao, R.; Tinnis, F.; Sun, J.; Siegbahn, P.E.M.; Andersson, P.G.; Åkermark, B. Catalytic water oxidation by a molecular ruthenium complex: Unexpected generation of a single-site water oxidation catalyst. *Inorg. Chem.* **2015**, *54*, 4611–4620. [[CrossRef](#)]
27. Meng, T.; Wang, H.; Zheng, Z.; Wang, K. pH-switchable Off-On-Off near-infrared luminescence based on a dinuclear ruthenium(II) complex. *Inorg. Chem.* **2017**, *56*, 4775–4779. [[CrossRef](#)]
28. Cheng, D.; Pan, Y.; Wang, L.; Zeng, Z.; Yuan, L.; Zhang, X. Selective visualization of the endogenous peroxynitrite in an inflamed mouse model by a mitochondria-targetable two-photon ratiometric fluorescent probe. *J. Am. Chem. Soc.* **2017**, *139*, 285–292. [[CrossRef](#)]
29. Cloonan, S.M.; Elmes, R.B.P.; Erby, M.L.; Bright, S.A.; Poynton, F.E.; Nolan, D.E.; Quinn, S.J.; Gunnlaugsson, T.; Williams, D.C. Detailed biological profiling of a photoactivated and apoptosis inducing pdppz ruthenium(II) polypyridyl complex in cancer cells. *J. Med. Chem.* **2015**, *58*, 4494–4505. [[CrossRef](#)]
30. Gao, Q.; Zhang, W.; Song, B.; Zhang, R.; Guo, W.; Yuan, J. Development of a novel lysosome-targeted ruthenium(II) complex for phosphorescence/time-Gated luminescence assay of biothiols. *Anal. Chem.* **2017**, *89*, 4517–4524. [[CrossRef](#)]
31. Hara, D.; Komatsu, H.; Son, A.; Nishimoto, S.; Tanabe, K. Water-soluble phosphorescent ruthenium complex with a fluorescent coumarin unit for ratiometric sensing of oxygen levels in living cells. *Bioconjugate Chem.* **2015**, *26*, 645–649. [[CrossRef](#)]
32. Sheet, S.K.; Sen, B.; Thounaojam, R.; Aguan, K.; Khatua, S. Ruthenium(II) complex-based luminescent bifunctional probe for Ag<sup>+</sup> and phosphate ions: Ag<sup>+</sup>-assisted detection and imaging of rRNA. *Inorg. Chem.* **2017**, *56*, 1249–1263. [[CrossRef](#)]
33. Gavrilova, A.L.; Bosnich, B. Principles of mononucleating and binucleating Ligand Design. *Chem. Rev.* **2004**, *104*, 349–384. [[CrossRef](#)] [[PubMed](#)]

34. Nakatani, K.; Sando, S.; Saito, I. Recognition of a single guanine bulge by 2-acylamino-1,8-naphthyridine. *J. Am. Chem. Soc.* **2000**, *122*, 2172–2177. [[CrossRef](#)]
35. Hooek, C.; Reichert, J.; Schmidtke, M. Fluorescent 1,7-dialkylamino-[1,8]-naphthyridines: Preparation and spectroscopic properties. *Molecules* **1999**, *4*, 264–271. [[CrossRef](#)]
36. Nakataniz, K.; Sando, S.; Kumasawa, H.; Kikuchi, J.; Saito, I. Recognition of guanine-guanine mismatches by the dimeric form of 2-amino-1,8-naphthyridine. *J. Am. Chem. Soc.* **2001**, *123*, 12650–12657. [[CrossRef](#)] [[PubMed](#)]
37. Vu, C.; Walker, D.D.; Wells, J.; Fox, S. Elaboration of 1,8-naphthyridine-2,7-dicarboxaldehyde into novel 2,7-dimethylimine Derivatives. *J. Heterocycl. Chem.* **2002**, *829*, 829–832. [[CrossRef](#)]
38. Cavanaugh, M.A.; Cappo, V.M.; Alexander, C.J.; Good, M.L. Substituted 1,8-naphthyridine complexes of iron(II) and iron(III). *Inorg. Chem.* **1976**, *11*, 2615–2621. [[CrossRef](#)]
39. Chandler, C.J.; Deady, L.W.; Reiss, J.A.; Tzimos, V. The synthesis of macrocyclic polyether-dieters incorporating 1,10-phenanthroline and 1,8-naphthyridino subunits. *J. Heterocycl. Chem.* **1982**, *19*, 1017–1019. [[CrossRef](#)]
40. Becke, A.D. Density-functional thermochemistry. III. The role of exact exchange. *J. Chem. Phys.* **1993**, *98*, 1372–1377. [[CrossRef](#)]
41. Sullivan, B.P.; Salmon, D.J.; Meyer, T.J. Monomeric and dimeric pyrazole and pyrazolyl complexes of ruthenium. *Inorg. Chem.* **1978**, *17*, 3334–3341. [[CrossRef](#)]
42. Best, Q.A.; Xu, R.S.; McCarrroll, M.E.; Wang, L.C.; Dyer, D.J. Design and investigation of a series of rhodamine-based fluorescent probes for optical measurements of pH. *Org. Lett.* **2010**, *12*, 3219–3221. [[CrossRef](#)]
43. Zhang, S.T.; Li, P.; Liao, C.; Luo, T.; Kou, X.; Xiao, D. A highly sensitive luminescent probe based on Ru(II)-bipyridine complex for Cu<sup>2+</sup>, l-histidine detection and cellular imaging. *Spectrochim. Acta Part A* **2018**, *201*, 161–169. [[CrossRef](#)] [[PubMed](#)]
44. Jiang, W.; Yang, S.; Lu, W.; Gao, B.; Xu, L.; Sun, X.; Jiang, D.; Xu, H.J.; Ma, M.; Cao, F. A novel fluorescence turn off-on nano-sensor for detecting Cu<sup>2+</sup> and Cysteine in living cells. *J. Photoch. Photobiol. A* **2018**, *362*, 14–20. [[CrossRef](#)]
45. Anbu, S.; Ravishankaran, R.; Guedes da Silva, M.F.C.; Karande, A.A.; Pombeiro, A.J. Differentially selective chemosensor with fluorescence off–on responses on Cu<sup>2+</sup> and Zn<sup>2+</sup> ions in aqueous media and applications in pyrophosphate sensing, live cell imaging, and cytotoxicity. *Inorg. Chem.* **2014**, *53*, 6655–6664. [[CrossRef](#)] [[PubMed](#)]
46. Cheng, F.; He, C.; Ren, M.; Wang, F.; Yang, Y. Two dinuclear Ru(II) polypyridyl complexes with different photophysical and cation recognition properties. *Spectrochim. Acta Part A* **2015**, *136*, 845–851. [[CrossRef](#)]
47. Liao, Q.; Li, A.; Li, Z.; Jiang, Y. 2-Amino-5-(p-dimethylamino) phenyl-1, 3, 4-thiadiazole selective fluorescent chemosensor for Hg<sup>2+</sup>. *Chem. J. Chin. U.* **2008**, *29*, 2531–2534.
48. Xu, J.; Liu, N.; Hao, C.; Han, Q.; Duan, Y.; Wu, J. A novel fluorescence on-off-on peptide-based chemosensor for simultaneous detection of Cu<sup>2+</sup>, Ag<sup>+</sup> and S<sup>2-</sup>. *Sens. Actuator B* **2019**, *280*, 129–137. [[CrossRef](#)]
49. Wang, L.; Qin, W.; Tang, X.; Dou, W.; Liu, W.; Teng, Q.; Yao, X. A selective, cell-permeable fluorescent probe for Al<sup>3+</sup> in living cells. *Org. Biomol. Chem.* **2010**, *8*, 3751–3757. [[CrossRef](#)]

**Sample Availability:** Samples of the compounds are available from the authors.



© 2019 by the authors. Licensee MDPI, Basel, Switzerland. This article is an open access article distributed under the terms and conditions of the Creative Commons Attribution (CC BY) license (<http://creativecommons.org/licenses/by/4.0/>).